A Global Sensitivity Analysis Framework for Hybrid Simulation

G Abbiati, S. Marelli, N Tsokanas, B. Sudret, B Stojadinovic

▶ To cite this version:

HAL Id: hal-02337030

https://hal.archives-ouvertes.fr/hal-02337030

Submitted on 29 Oct 2019

ETH*zürich*

A Global Sensitivity Analysis Framework for Hybrid Simulation

G. Abbiati, S. Marelli, N. Tsokanas, B. Sudret, B. Stojadinovic

Chair of Risk, Safety and Uncertainty Quantification
Stefano-Franscini-Platz 5
CH-8093 Zürich

Data Sheet

A Global Sensitivity Analysis Framework for Hybrid Simulation

G. Abbiati, S. Marelli, N. Tsokanas, B. Sudret, B. Stojadinovic

October 1, 2019

Abstract

Hybrid Simulation is a dynamic response simulation paradigm that merges physical experiments and computational models into a hybrid model. In earthquake engineering, it is used to investigate the response of structures to earthquake excitation. In the context of response to extreme loads, the structure, its boundary conditions, damping, and the ground motion excitation itself are all subjected to large parameter variability. However, in current seismic response testing practice, Hybrid Simulation campaigns rely on a few prototype structures with fixed parameters subjected to one or two ground motions of different intensity. While this approach effectively reveals structural weaknesses, it does not reveal the sensitivity of structure's response. This thus far missing information could support the planning of further experiments as well as drive modeling choices in subsequent analysis and evaluation phases of the structural design process.

This paper describes a Global Sensitivity Analysis framework for Hybrid Simulation. This framework, based on Sobol' sensitivity indices, is used to quantify the sensitivity of the response of a structure tested using the Hybrid Simulation approach due to the variability of the prototype structure and the excitation parameters. Polynomial Chaos Expansion is used to surrogate the hybrid model response. Thereafter, Sobol' sensitivity indices are obtained as a by-product of polynomial coefficients, entailing a reduced number of Hybrid Simulations compared to a crude Monte Carlo approach. An experimental verification example highlights the excellent performance of Polynomial Chaos Expansion surrogates in terms of stable estimates of Sobol' sensitivity indices in the presence of noise caused by random experimental errors.

Keywords: Hybrid simulation, global sensitivity analysis, Sobol' indices, surrogate modeling, polynomial chaos expansion.

1 Introduction

Background and motivation   Hybrid Simulation (HS) is a dynamic simulation paradigm that merges physical experiments and computational models into a hybrid model. In mechanical and electrical engineering, such an approach is known as hardware-in-the-loop simulation. In earthquake engineering, hybrid simulation is used to investigate the behavior and eventual failure of a structure in response to extreme earthquake excitation. In detail, HS is conducted using a hybrid model, which combines physical and numerical substructures (NS and PS, respectively) that interact with each other in a real-time control loop, to simulate the time history response of a prototype structure subjected to a realistic excitation. The PS is tested in the laboratory using servo-controlled actuators equipped with force and displacement transducers. The NS is numerically simulated to avoid testing of those substructures that can be reliably replaced by numerical models (e.g., masses or components whose response remains in an easy-to-simulate range) or would exceed the testing capacities of the experimental facility. A real-time software ensures interface force balance and displacement compatibility between NS and PS by solving the equation of motion of the prototype structure online, that is, while structural testing is performed. As a result, HS reproduces the time history response of the prototype structure subjected to a realistic excitation. When the PS response is rate-independent, it is good practice to perform HS with an extended time scale from 50 to 200 times slower than real-time in order to improve control accuracy. Time scaling and testing of geometrically scaled substructures also drastically reduce the costs of HS compared to full-scale experimentation. The seminal report by Schellenberg and Mahin Shellenberg A.H. (2009) provides a comprehensive overview of state-of-art HS methods and algorithms.

HS is suitable either to investigate the behavior of a prototype structure at the system level, where PSs replace components lacking validated numerical models, or to observe the component-level behavior of PSs exposed to a realistic excitation, which includes dynamic interaction with possibly multiple NSs. The overarching goal is to support the validation and calibration of computer models Bursi et al. (2017). A system-level focus is pursued in earthquake engineering, where HS is preferred to shake table experiments for testing large structures such as bridges (e.g., Terzic et al. (2014)) and buildings (e.g., Christenson et al. (2008)). Similarly, testing of floating platforms with a sizeable scaling factor in hydrodynamic laboratories is challenging due to the extent of mooring line footprints, which can range from two to four times the water depth. For this reason, HS has been recently proposed to truncate mooring lines whose missing parts are simulated as NSs Sauder et al. (2018). A component-level focus is pursued in fire

engineering, where hybrid fire testing, the adaptation of HS to fire loading, originated in response to limitations of standard fire tests Whyte et al. (2016). The latter consists of exposing a single structural component to a predefined time-temperature loading curve inside a furnace and indeed does not account for the redistribution of internal forces caused, for example, by thermal expansion or partial collapse. For a similar motivation, Franza and Marshall Franza and Marshall (2018) developed an HS platform to study soil-structure interaction problems where a numerical model of a building frame (i.e., the NS) is used to mimic a realistic structural loading exerted on the physical centrifuge model of a tunnel-soil-foundation system (i.e., the PS). The use of HS in other engineering and science disciplines is growing (e.g. Vasmel et al. (2013), Becker et al. (2018)).

In earthquake engineering, which is the main field of expertise of some of the authors, boundary conditions, damping, and ground motion are all subjected to large parameter variability Bradley (2013). However, in the current experimental earthquake engineering practice, HS campaigns rely on a few prototype structures with fixed parameters subjected to one or two ground motions of different intensity. This testing procedure efficiently identifies the weaknesses of the tested prototype that could lead to the collapse of real structures in earthquakes. However, such a truncated procedure is indeed not adequate to estimate the *structural sensitivity* of the prototype structure response, i.e. quantifying the fraction of the variability of a generic response quantity of interest (QoI) due to the variability of each of the input parameters. This thus far missing information could support the planning of further experiments as well as drive modeling choices in subsequent analysis and evaluation phases of the structural design process.

Scope This paper describes a Global Sensitivity Analysis (GSA) framework for Hybrid Simulation that is intended to quantify the fraction of the variability of a generic response QoI of the prototype structure, evaluated via HS, due to the variability of a set of input variables that provide a suitable parametrization of the prototype structure and the excitation. Among the many GSA options, *Sobol' sensitivity indices*, a class of variance-decomposition-based methods Saltelli et al. (2007), were selected. Methods of this class rely upon the decomposition of the variance of a QoI as a sum of contributions of each input variable taken singularly or in combination with others. Unlike regression-based methods, variance-based methods do not require any kind of linearity or monotonicity of the functional relationship between input variables and QoIs.

An efficient way to compute Sobol' indices, originally introduced by Sudret Sudret (2008); Le Gratiet et al. (2017), is by post-processing the coefficients of a Polynomial Chaos Expansion

(PCE) of the QoI. PCE is a spectral decomposition method that projects the model response onto a functional basis of orthonormal multivariate polynomials in the input variables Xiu and Karniadakis (2002); Berveiller et al. (2006). Once the PCE representation is available, Sobol' indices are readily available by simply post-processing polynomial coefficients with no additional computational cost. The strategies for the calculation of the PCE can be broadly classified into two approaches: i) intrusive i.e., schemes that require the knowledge and adaptation of the governing equations of the model; and ii) non-intrusive i.e., schemes that (repeatedly) utilize the model to compute an outcome without modifying the model itself, which is considered as a *black-box*. HS and its PSs, and experimental testing in general, imply a non-intrusive PCE strategy. Hence, in this paper, the sparse adaptive least-square minimization based on Least Angle Regression (LAR) Blatman and Sudret (2011) was adopted. The proposed GSA framework for HS is illustrated using a case study based on a 3-degrees-of-freedom (3-DoFs) prototype structure excited by earthquake ground motions. HSs are performed using a 3-DoFs HS test rig installed at the Structural Laboratory of ETH Zurich. The GSA of the prototype structure response is performed for two response QoIs against four input variables, which parametrize both the NS and the excitation.

The paper is organized as follows. Section 2 describes the GSA framework based on PCE. Section 3 describes the case study, including a detailed description of the HS setup and the HSs. Section 4 presents the results of the GSA of the prototype structure response. Finally, conclusions and future outlook are given.

2   Global Sensitivity Analysis framework

Let us denote with $\mathbf{X} = \{X_1, \ldots, X_M\}$ an M-dimensional vector of input variables to parametrize the NSs, the PSs and the excitation (or a subset of these) of the hybrid model of the prototype structure, and with Y a generic response QoI of the prototype structure evaluated via HS of the response of the hybrid model. A mapping $\mathcal{M}$ between input variables and a single QoI reads,

$$\mathbf{X} \in \mathcal{D}_{\mathbf{X}} \subset \mathbb{R}^M \mapsto Y = \mathcal{M}(\mathbf{X}) \subset \mathbb{R} \tag{1}$$

It can be argued that the inherent variability of the response of different samples corresponding to nominally identical PSs of the hybrid model, as well as measurement noise during HS, which both propagate through to the hybrid model response QoI, requires a stochastic mapping between input variables and QoIs. However, the scope of this paper is limited to the case of PSs with almost deterministic behavior. Moreover, relevant studies testify that measurement noise of

4

standard structural testing equipment has a negligible effect on the prototype structure response evaluated via HS Ahmadizadeh and Mosqueda (2009); Abbiati et al. (2018). Therefore, $\mathcal{M}$ is assumed to be deterministic. Since our target is to estimate the *structural sensitivity* of the prototype structure response, which means quantifying the fraction of the variability of a generic QoI due to the variability of the input variables, all input variables in $\mathbf{X}$ are assumed to be statistically independent and uniformly distributed. The finite bounds of input variables compatible with force and displacement ranges allowed by the experimental facility are the only constraints of $\mathbf{X}$.

2.1 Sobol'-Hoeffding decomposition and sensitivity indices

Assume that the vector of input variables $\mathbf{X}$ has support $\mathcal{D}_{\mathbf{X}}$ and follows an independent joint probability density function (PDF) $f_{\mathbf{X}}(\mathbf{x}) = \prod_i^M f_{X_i}(x_i)$ where f_{X_i} is the marginal PDF of the i-th input variable. Any square-integrable mapping $Y = \mathcal{M}(\mathbf{X})$ with respect to the probability measure associated with $f_{\mathbf{X}}$, can be written as a sum of functions of increasing dimension as Sobol' (1993):

$$\mathcal{M}(\mathbf{X}) = \mathcal{M}_0 + \sum_{i=1}^{M} \mathcal{M}_i(X_i) + \sum_{1 \le i \le j \le M} \mathcal{M}_{i,j}(X_i, X_j) + \ldots + \mathcal{M}_{1,2,\ldots,M}(\mathbf{X}), \tag{2}$$

or equivalently:

$$\mathcal{M}(\mathbf{X}) = \mathcal{M}_0 + \sum_{\mathbf{u} \ne \emptyset} \mathcal{M}_{\mathbf{u}}(\mathbf{X}_{\mathbf{u}}), \tag{3}$$

where $\mathcal{M}_0$ is the mean value of Y, $\mathbf{u} = \{i_1, \ldots, i_s\} \subset \{1, \ldots, M\}$ are index sets, and $\mathbf{X}_{\mathbf{u}}$ denotes a subvector of $\mathbf{X}$ containing only the components indexed by $\mathbf{u}$. The number of summands in the above equation is $2^M - 1$. The Sobol' decomposition is unique under the condition:

$$\int_{\mathcal{D}_{X_k}} \mathcal{M}_{\mathbf{u}}(\mathbf{x}_{\mathbf{u}}) f_{X_k}(x_k) \, dx_k = 0 \text{ , if } k \in \mathbf{u}, \tag{4}$$

where $\mathcal{D}_{X_k}$ and f_{X_k} denote the support and marginal PDF of X_k, respectively, which leads to the orthogonality property:

$$\mathbb{E}\left[\mathcal{M}_{\mathbf{u}}(\mathbf{x}_{\mathbf{u}}) \cdot \mathcal{M}_{\mathbf{v}}(\mathbf{x}_{\mathbf{v}})\right] = 0 \text{ , if } \mathbf{u} \ne \mathbf{v}. \tag{5}$$

The uniqueness and orthogonality properties allow for the following decomposition of the variance D of Y:

$$D = \text{Var}\left[\mathcal{M}(\mathbf{X})\right] = \sum_{\mathbf{u} \ne \emptyset} \mathcal{D}_{\mathbf{u}} \tag{6}$$

where $\mathcal{D}_{\mathbf{u}}$ denotes the partial variance:

$$\mathcal{D}_{\mathbf{u}} = \mathrm{Var}\left[\mathcal{M}_{\mathbf{u}}\left(\mathbf{x}_{\mathbf{u}}\right)\right] = \mathbb{E}\left[\mathcal{M}_{\mathbf{u}}^2\left(\mathbf{x}_{\mathbf{u}}\right)\right]. \tag{7}$$

The Sobol' index $S_{\mathbf{u}}$ can be defined as the fraction of the total variance $D_{\mathbf{u}}$ that corresponds to the set of input variables indexed by $\mathbf{u}$:

$$S_{\mathbf{u}} = \frac{D_{\mathbf{u}}}{D}. \tag{8}$$

By construction, $\sum_{\mathbf{u}\neq\emptyset} S_{\mathbf{u}} = 1$. First-order indices $S_i^{(1)}$ describe the influence of each parameters X_i considered separately. Second-order indices $S_{ij}^{(2)}$ describe the influence from pairs of parameters $\{X_i, X_j\}$ not already accounted for by X_i or X_j separately. High-order indices describe combine influences from larger sets of parameters. The total sensitivity indices $S_i^{(\mathrm{tot})}$ represent the total effect of an input variable X_i accounting for its main effect and all interactions with other input variables. It follows that $S_i^{(\mathrm{tot})} = 1 - S_{\sim i}$, where $S_{\sim i}$ is the sum of all $S_{\mathbf{u}}$ with $\mathbf{u}$ not including i. Sobol' indices can be evaluated by Monte Carlo simulation (Saltelli et al., 2007), which requires $\mathcal{O}(10^3)$ model evaluations for each index $S_{\mathbf{u}}$. Clearly, this is not affordable when each evaluation of $\mathcal{M}(\mathbf{x})$ entails the execution of a HS. On the other hand, when the PCE of the QoI is available, Sobol' indices can be obtained analytically at no additional cost. A concise description of PCE-based Sobol' sensitivity indices estimation is given in the following section; for further details, the reader is referred to Sudret (2008); Le Gratiet et al. (2017).

2.2 Sobol' indices from Polynomial Chaos Expansion

Sparse PCE Blatman and Sudret (2011) is a well-known surrogate modeling technique. Its close relation to Sobol' variance decomposition Sudret (2008) together with good denoising performance Torre et al. (2019) make sparse PCE ideal to surrogate the prototype structure response evaluated via HS. PCE relies on the decomposition of a random model response QoI $Y = \mathcal{M}(\mathbf{X})$ as a linear superposition of non-linear functions as follows:

$$\widehat{Y} = \mathcal{M}^{\mathrm{PCE}}\left(\mathbf{X}\right) = \sum_{\boldsymbol{\alpha}\in\mathcal{A}} y_{\boldsymbol{\alpha}}\Psi_{\boldsymbol{\alpha}}\left(\mathbf{X}\right), \tag{9}$$

where $\{\Psi_{\boldsymbol{\alpha}}, \boldsymbol{\alpha}\in\mathcal{A}\}$ is a set of multivariate polynomials that are orthogonal with respect to the input vector with independent components $\mathbf{X} \sim f_{\mathbf{X}}(\mathbf{x}) = \prod_{i=1}^M f_{\mathbf{X}_i}(\mathbf{x}_i)$, $\boldsymbol{\alpha} = (\alpha_1, \ldots \alpha_M)$ is a multi-index that identifies the polynomial degree in each of the input variables, and $y_{\boldsymbol{\alpha}}$ denotes the corresponding polynomial coefficient (coordinate). Following the orthonormality condition, $\mathbb{E}\left[\mathcal{M}^{\mathrm{PCE}}\left(\mathbf{X}\right)\right] = y_{\mathbf{0}}$. For practical purposes, the infinite sum in (9) needs to be truncated to a finite series. This is commonly achieved by maximum-degree or hyperbolic norm truncation (for

more details, see Blatman and Sudret (2011)). In this paper, a sparse least-square regression for the estimation of the set of coefficients $\mathbf{y} = \{y_{\boldsymbol{\alpha}}, \boldsymbol{\alpha} \in \mathcal{A}\}$ is adopted Blatman and Sudret (2011).

A so-called *experimental design* (ED), consisting of a set of realization of the input vector $\mathcal{X} = \{\mathbf{x}^{(1)}, \ldots, \mathbf{x}^{(N)}\}$ and the corresponding model evaluations $\mathcal{Y} = \{y^{(1)}, \ldots, y^{(N)}\}$, is generated first using repeated HS. In a second step, the set of coefficients $\mathbf{y}_{\alpha}$ is estimated by minimizing the expected mean-square approximation error on the ED by solving:

$$\widehat{\mathbf{y}}_{\alpha} = \underset{\mathbf{y}_{\alpha}}{\arg \min} \, \mathbb{E}\left[\left(Y - \widehat{Y}\right)^2\right] \tag{10}$$

In the present application, the ED was formed by sampling the input variable space with a Sobol' low-discrepancy sequence. The minimization in (10) was solved using the hybrid LAR method originally proposed in Blatman and Sudret (2011). A good measure of the accuracy of PCE is the mean-square residual error $Err_G = \mathbb{E}\left[\left(Y - \widehat{Y}\right)^2\right]$, often simply referred to as *generalization error*. However, the evaluation of Err_G would require an additional validation data set, which is typically unavailable. It is thus desirable to obtain an estimate of Err_G using only the information included in the ED.

One such error estimation method is the co-called leave-one-out cross-validation error (LOO). Denote by $\mathcal{M}^{PCE \setminus i}$ the PCE built from the subset of the ED obtained by removing the pair $\{\mathbf{x}^{(i)}, y^{(i)}\}$. The LOO error is defined as:

$$\epsilon_{LOO} = \frac{1}{N} \sum_{i=1}^{N} \left[\mathcal{M}\left(\mathbf{x}^{(i)}\right) - \mathcal{M}^{PCE \setminus i}\left(\mathbf{x}^{(i)}\right)\right]^2. \tag{11}$$

In the case of regression-based PCE, ϵ_{LOO} can be calculated directly from the coefficients of the PCE computed with the *entire* ED, without explicitly solving (10) multiple times Berveiller et al. (2006). This robust error estimate allows one to devise basis-adaptive PCE schemes. A truncation scheme can be gradually relaxed, e.g. by increasing the maximum polynomial degree, until some convergence criterion on ϵ_{LOO} is achieved Blatman and Sudret (2011). Due to the rapid convergence of the sparse PCE coefficients, this approach provides a very efficient means to propagate the variability in the input variables to QoIs without the need for several evaluations of the model response otherwise required by standard MC techniques.

It is straightforward to obtain the Sobol' decomposition of Y in an analytical form by observing that the summands $\mathcal{M}_{\mathbf{u}}^{\text{PCE}}(\mathbf{X}_{\mathbf{u}})$ in (3) can be written as:

$$\mathcal{M}_{\mathbf{u}}^{\text{PCE}}(\mathbf{X}_{\mathbf{u}}) = \sum_{\boldsymbol{\alpha} \in \mathcal{A}_{\mathbf{u}}} y_{\boldsymbol{\alpha}} \boldsymbol{\Psi}_{\boldsymbol{\alpha}}(\mathbf{X}_{\mathbf{u}}), \tag{12}$$

where $\mathcal{A}_{\mathbf{u}}$ denotes the set of multi-indices that depend only on $\mathbf{u}$:

$$\mathcal{A}_{\mathbf{u}} = \{\boldsymbol{\alpha} \in \mathcal{A} : \alpha_k \neq 0 \text{ if and only if } k \in \mathbf{u}\} \tag{13}$$

Clearly, $\cup \mathcal{A}_{\mathbf{u}} = \mathcal{A}$. Consequently, due to the uniqueness of Sobol'-Hoeffding decomposition, there is an analytical expression of $\mathcal{M}_{\mathbf{u}}^{\mathrm{PCE}}$ (12), which serves as a proxy of $\mathcal{M}_{\mathbf{u}}$. Due to the orthogonality of the basis, the total variance of a PCE is analytically given by Xiu and Karniadakis (2002):

$$D = \mathrm{Var}\left[\mathcal{M}^{\mathrm{PCE}}\left(\mathbf{X}\right)\right] = \sum_{\boldsymbol{\alpha} \in \mathcal{A}} y_{\boldsymbol{\alpha}}^2. \tag{14}$$

Similarly, the partial variance $D_{\mathbf{u}}$ reads:

$$D_{\mathbf{u}} = \mathrm{Var}\left[\mathcal{M}_{\mathbf{u}}^{\mathrm{PCE}}\left(\mathbf{X_u}\right)\right] = \sum_{\boldsymbol{\alpha} \in \mathcal{A}_{\mathbf{u}}} y_{\boldsymbol{\alpha}}^2. \tag{15}$$

Accordingly, the Sobol' indices of any order can be approximated by a simple combination of the squares of the PCE coefficients by substituting (15) and (14) in (8). For instance, the first-order Sobol' indices, which describe the influence of each input variable X_i considered separately, read:

$$S_i^{(1)} = \frac{\sum\limits_{\boldsymbol{\alpha} \in \mathcal{A}_i} y_{\boldsymbol{\alpha}}^2}{\sum\limits_{\boldsymbol{\alpha} \in \mathcal{A}} y_{\boldsymbol{\alpha}}^2} \ , \ \mathcal{A}_i = \{\boldsymbol{\alpha} \in \mathcal{A} : \alpha_i > 0 \ , \ \alpha_{i \neq j} = 0\} \tag{16}$$

whereas the total Sobol' indices, which represent the total effect of an input variable X_i accounting for its main effect and all interaction with other input variables, are given by:

$$S_i^{(\mathrm{tot})} = \frac{\sum\limits_{\boldsymbol{\alpha} \in \mathcal{A}_i^{\mathrm{tot}}} y_{\boldsymbol{\alpha}}^2}{\sum\limits_{\boldsymbol{\alpha} \in \mathcal{A}} y_{\boldsymbol{\alpha}}^2} \ , \ \mathcal{A}_i^{\mathrm{tot}} = \{\boldsymbol{\alpha} \in \mathcal{A} : \alpha_i > 0\}. \tag{17}$$

Sobol' indices provide quantitative insight on the importance of an input variable. However, they do not include information about the direction in which an input variable affects the QoI. So-called univariate effects can answer this question (Deman et al., 2016; Harenberg et al., 2019). A univariate effect is the expectation of a QoI conditioned to the value of a single input variable. Univariate effects have a closed analytical form for PCE models, which is closely related to the first-order Sobol' decomposition:

$$\mathcal{M}_i^{(1)}\left(X_i\right) = \sum_{\boldsymbol{\alpha} \in \mathcal{A}_i} y_{\boldsymbol{\alpha}} \Psi_{\boldsymbol{\alpha}}\left(X_i\right) \ , \ \mathcal{A}_i = \{\boldsymbol{\alpha} \in \mathcal{A} : \alpha_i > 0, \alpha_{i \neq j} = 0\} \tag{18}$$

In this paper, computations of both PCE and Sobol' indices are performed using UQLab, which is a MATLAB toolbox for uncertainty quantification developed by the Chair of Risk, Safety and Uncertainty Quantification of ETH Zurich Marelli and Sudret (2014, 2019); Marelli et al. (2019).

3 Case study

In order to provide experimental validation of the proposed GSA framework for HS, a case study was conducted using a 3-DoFs prototype structure subjected to earthquake ground motion

excitation.

3.1 Prototype structure and excitation

The prototype structure consists of a simply-supported massive beam coupled at the ends to two linear-elastic rotation restraints, two lumped masses, and one dashpot. The beam is subjected to a ground motion excitation $a_g(t)$ acting in the direction orthogonal to its axis. Bending and axial deformation of the beam are coupled for large displacements, which means that the prototype structure is characterized by a geometrical nonlinearity. Figure 1 provides a schematic view of the prototype structure and its hybrid model substructured into one PS and two NS for the purpose of HS.

(a)

(b)
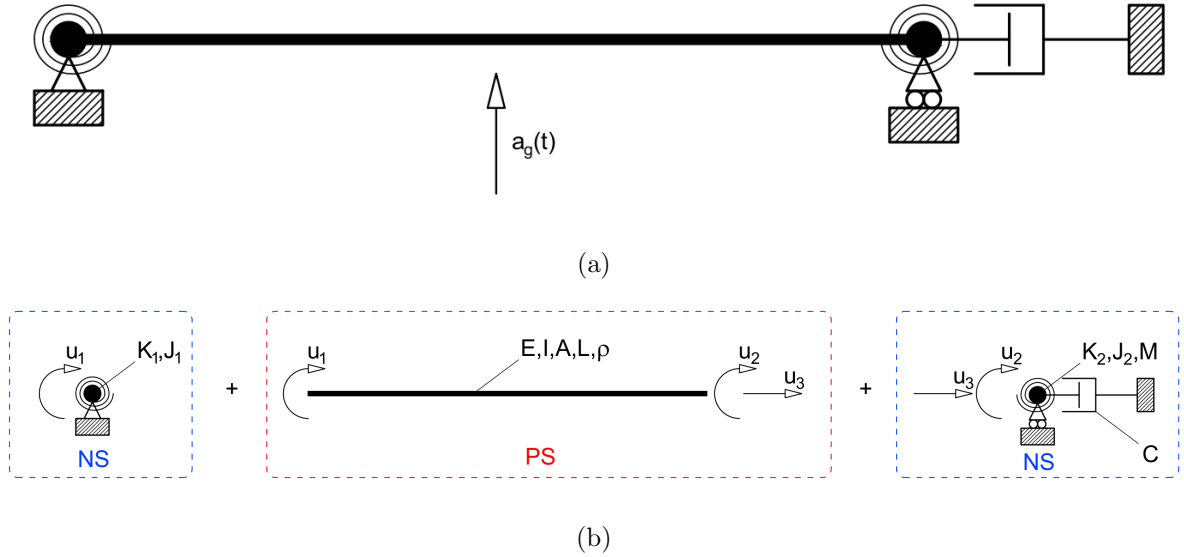
Figure 1: Case study: (a) prototype structure; (b) hybrid model comprising two NS and one PS.

In Figure 1 u_1 and u_2 indicate the two rotational DoFs of the simply-supported beam, while u_3 corresponds to its axial DoF. The PS is instantiated using a $L = 470\,\mathrm{mm}$ long iron plate (Young modulus $E = 100$ GPa, density $\rho = 7850\,\frac{kg}{m^3}$), with a $200 \times 2\,\mathrm{mm}$ cross-section (area $A = 400\,mm^2$ and moment of inertia $I = 133\,mm^4$). Since HSs are conducted with a testing time scale equal to 50, a numerical mass matrix accounts for the PS inertia. In detail, the PS mass matrix is estimated by condensing the six-by-six consistent mass matrix of a two-dimensional Bernoulli beam element to the three DoFs retained by the hybrid model. The out-of-diagonal entries of the reduced mass matrix couple the inertial acceleration of the ground motion to the

rotation DoFs of the hybrid model. The NS of the hybrid model comprises two rotational masses $J_1 = J_2 = 0.9\,kgm^2$, a translation mass $M = 20,000\,kg$ all lumped at the supports. The linear dash-pot with a damping coefficient $C = 300,000\,\frac{Ns}{m}$ is the only source of numerical damping and prevents the excitation of the axial eigenmode of the hybrid model. The two linear elastic rotation springs, whose stiffness K_1 and K_2 are defined as input variables for GSA, represent the non-deterministic properties of the prototype structure supports.

The velocity-pulse model proposed by Dabaghi and Der Kiureghian (2018), which describes near-field earthquake ground motions, defines the excitation $a_g(t)$. The velocity-pulse model consists of a cosine carrier wave with a period T_p, modulated by a truncated cosine function, namely the pulse function, with a period γT_p and amplitude V_p. The latter corresponds to the peak velocity of the pulse occurring at time $t_{max,p}$. The expression for the velocity-pulse reads:

$$v_g(t) = \left(\frac{V_p}{2} \cos \left(2\pi \left(\frac{t - t_{max,p}}{T_p} \right) + \nu \right) - \frac{D_r}{\gamma T_p} \right) \left(1 + \cos \left(\frac{2\pi}{\gamma} \left(\frac{t - t_{max,p}}{T_p} \right) \right) \right), \qquad (19)$$

where ν is the phase angle between the cosine wave and pulse function, while D_r is the non-zero residual displacement at the end of the pulse, which is in turn given by:

$$D_r = V_p T_p \frac{\sin\left(\nu + \gamma\pi\right) - \sin\left(\nu - \gamma\pi\right)}{4\pi\left(1 - \gamma^2\right)}. \qquad (20)$$

The transverse inertial acceleration $a_g(t)$ applied to the prototype structure corresponds to the time derivative of the velocity-pulse model. The velocity-pulse model is defined for $t \in \{0, \gamma T_p\}$ and is zero outside this interval. In order to reduce the number of free parameters, the velocity pulse peak is located at $t_{max,p} = \frac{\gamma T_p}{2}$ and $\gamma = 2$ and $\nu = 0.1$. Thus, pulse peak velocity V_P and period T_P are selected as input variables for GSA. Figure 2 depicts a realization of the velocity-pulse model described by (19) and (20) with $V_P = 2\,\frac{m}{s}$, $T_P = 1.25\,s$, $\gamma = 2.0$ and $\nu = 0.1\,rad$.

The GSA of the hybrid model is evaluated using two response QoIs, $u_{1,\mathrm{max}}$, the maximum absolute rotation at the left support of the beam measured using the vertical actuator displacement, and $r_{1,\mathrm{max}}$, the maximum absolute bending moment at the left support of the beam measured using the vertical actuator load cells, as depicted in Figure 1. Following the notation introduced in Section 2, the vector of input variables and the vector of QoIs read:

$$\begin{aligned} \mathbf{X} &= \{V_P, T_P, K_1, K_2\} \\ \mathbf{Y} &= \{u_{1,\mathrm{max}}, r_{1,\mathrm{max}}\} \end{aligned} \qquad (21)$$

The input variables are assumed to be uniformly distributed. The values of the input variables are constrained to intervals reported in Table 1 to comply with the physical limits of the HS
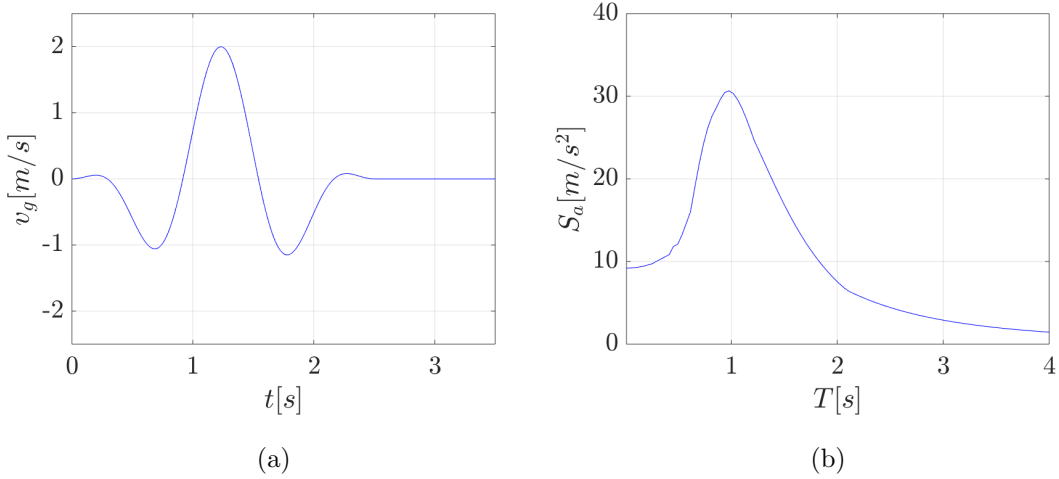
Figure 2: Sample excitation used in the case study: (a) Velocity-pulse time history, and (b) the corresponding acceleration response spectrum S_a computed using a 5% damping ratio.

Table 1: Input variable intervals and assumed probability distributions.

Parameter	Probability distribution	Lower bound	Upper bound	Unit
K_1	Uniform	20	120	$\left[\frac{Nm}{rad}\right]$
K_2	Uniform	20	120	$\left[\frac{Nm}{rad}\right]$
V_p	Uniform	1.00	3.00	$\left[\frac{m}{s}\right]$
T_p	Uniform	0.50	2.00	$[s]$

test setup as well as to avoid yielding and permanently deforming the PS. Accordingly, the same steel plate was used as the PS in the entire case study. If $K_1 = K_2$ and both vary within the range proposed in Table 1, the period of the first bending mode of the prototype structure ranges between 0.68 and 0.45 s. This range overlaps with the period range of the carrier signal of the velocity-pulse excitation, which varies between 0.50 and 2.00 s. Accordingly, the variable frequency tuning between the excitation and the first bending eigenmode of the hybrid model is expected to affect the dynamic amplification of both response QoIs.

3.2   Hybrid simulation setup

The 3-DoFs HS test rig used to conduct the HSs is a stiff loading frame equipped with four electro-mechanical actuators interfaced to an INDEL real-time computer Abbiati et al. (2018). The 3-DoFs HS test rig is designed to test plate specimens with an approximate footprint of
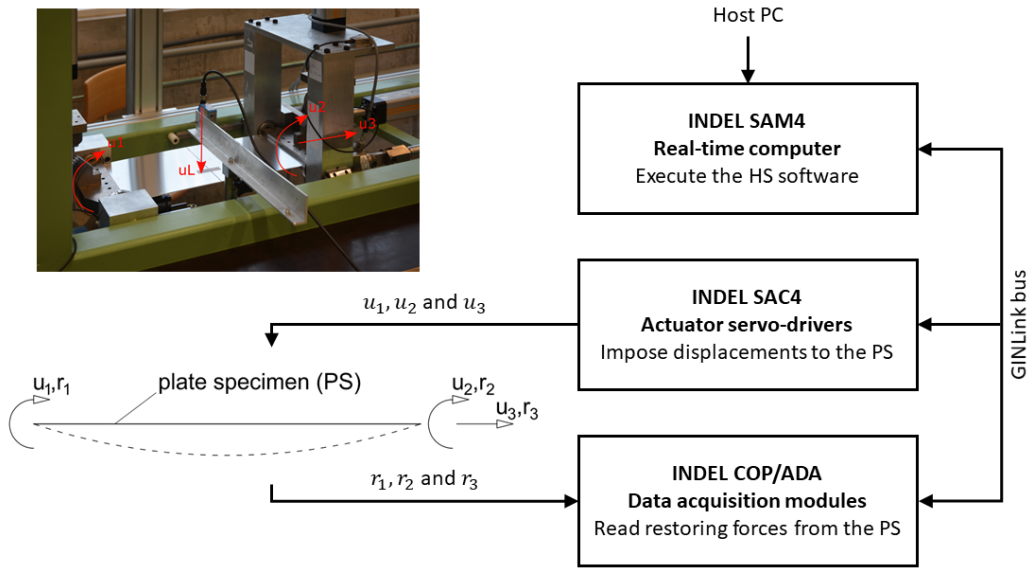
11

Figure 3: Architecture of the 3-DoFs HS test rig.

200×500 mm and thickness varying between 1 and 3 mm. Figure 3 illustrates the architecture of the HS setup, including a close-up view of the plate specimen accommodation. The GINLink bus connects the actuator servo-driver INDEL SAC4 and all data acquisition modules INDEL COP-ADA to the real-time computer INDEL SAM4, which runs the HS software. The latter is developed in the MATLAB/SIMULINK environment and downloaded to the real-time computer INDEL SAM4 via Ethernet from the Host-PC. At each simulation time step, the HS software imposes displacements u_1, u_2 and u_3 to the plate specimen, the PS, reads the corresponding restoring forces r_1, r_2 and r_3 measured using force transducers, and solves the coupled equation of motion of the hybrid model. In addition, a laser sensor measures the out-of-plane deflection at the mid-span of the plate specimen (labeled UL in Figure 3). A detailed description of the time integration scheme adopted to solve the equation of motion is reported in the appendix of this paper. Figure 4 shows two axonometric views of the 3-DoFs HS test rig, including the main hardware components. In this figure, grey parts are fixed to the reaction frame, which is not visible, while the moving parts of the 3-DoF HS test rig are colored in yellow. The two rack-pinion systems (10) convert motion along the vertical actuator axes y_1 and y_2 (1) to rotations u_1 and u_2, respectively, which are imposed to the short edges of the plate specimen (6) through aluminum clamps (3). Horizontal actuators along axes x_1 and x_2 (2) control the position of the moving frame (4), which is mounted on two profiled rail guides using ball bearings (5). As a
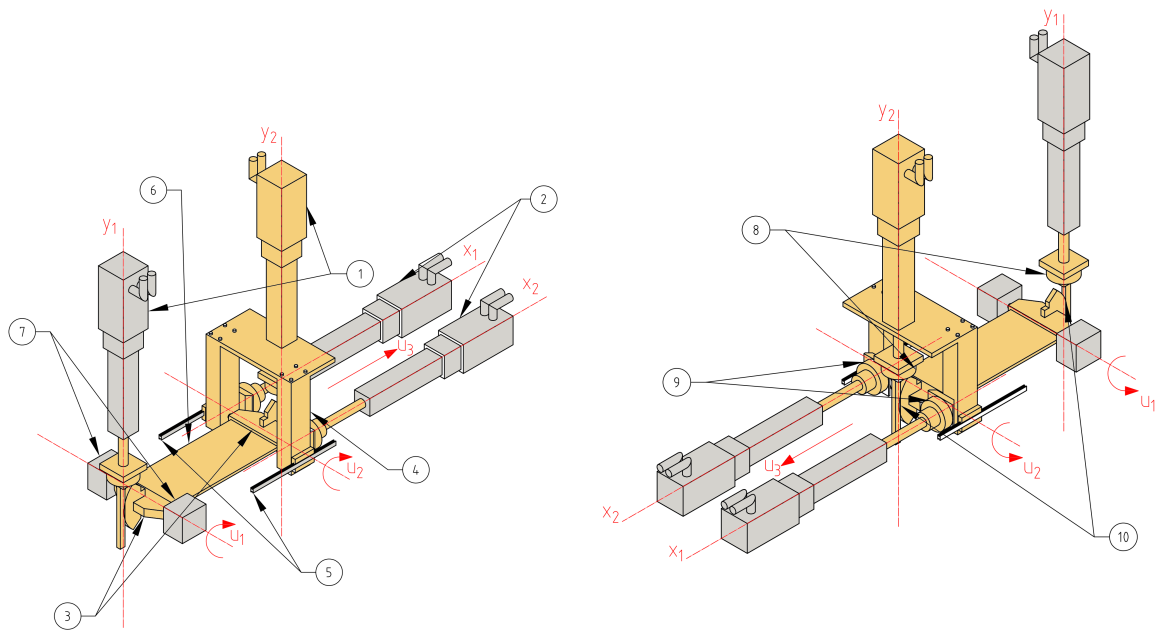
Figure 4: Axonometric views of the 3-DoFs HS test rig with main components: (1) vertical actuators; (2) horizontal actuators; (3) installation clamps; (4) moving frame; (5) profiled rail guides; (6) plate specimen; (7) hinges; (8) vertical actuator load cells; (9) horizontal actuator load cells; (10) rack-pinion systems. The moving parts are colored in yellow while the grey parts are fixed to the reaction frame, which is omitted in this figure for clarity.

result, the position of the moving frame (4) equals the axial elongation of the plate specimen u_3 (6).

4 Case study results

This section reports the results of the case study where the GSA procedure described in Section 2 was employed to evaluate and quantify the sensitivities of the response of the prototype structure defined in Section 3 to earthquake ground motion excitation using the results of a number of HS conducted using the 3-DoFs test rig described in Section 3.

4.1 Surrogate modeling using PCE

Based on the input variable intervals and distributions specified in Table 1, a Sobol' sequence was used to generate 200 samples of the input variable vector $\mathbf{X}$. For each of these samples, a HS of the response of the hybrid model (Figure 1) of the prototype structure to a velocity-pulse ground motion excitation was conducted to determine the time history of the response QoIs in vector $\mathbf{Y}$. An outcome of a sample HS of the response of the prototype structure with support rotation spring stiffness $K_1 = K_2 = 70\,\mathrm{Nm/rad}$ to the velocity pulse shown in Figure 2 in terms of time histories of the rotation $u_1(t)$ and moment $r_1(t)$ is reported in Figure 5, where the corresponding peak response QoIs $u_{1,\max}$ and $r_{1,\max}$ are also highlighted. According to the procedure outlined in Section 2.2, ED was used to train the PCEs of response QoI $u_{1,\max}$ and $r_{1,\max}$.

The time history response of r_1 is much noisier than that of u_1. This is a common occurrence with easily deformable specimens that produce low reaction forces for appreciable displacements, emphasizing the random measurement errors made by the load cells designed for higher loads. Accordingly, more random fluctuations are expected on $r_{1,\max}$ than on $u_{1,\max}$, which negatively affect the convergence of the corresponding PCE. This is confirmed by Figure 6, which shows the relationship between QoI measurements and corresponding PCE estimates for both QoIs. In detail, blue squares refer to the validation of PCEs trained on the entire ED made of 200 samples, whereas red circles refer to cross-validation PCEs. In the latter case, four PCEs were trained on four different ED subsets of 150 samples each, evaluated on the remaining 50 samples, and compared to corresponding measurements.

Figure 6 further shows that validation and cross-validation scatter plots for the same QoI have similar dispersion. This means that an ED of 150 samples is sufficient to achieve stable
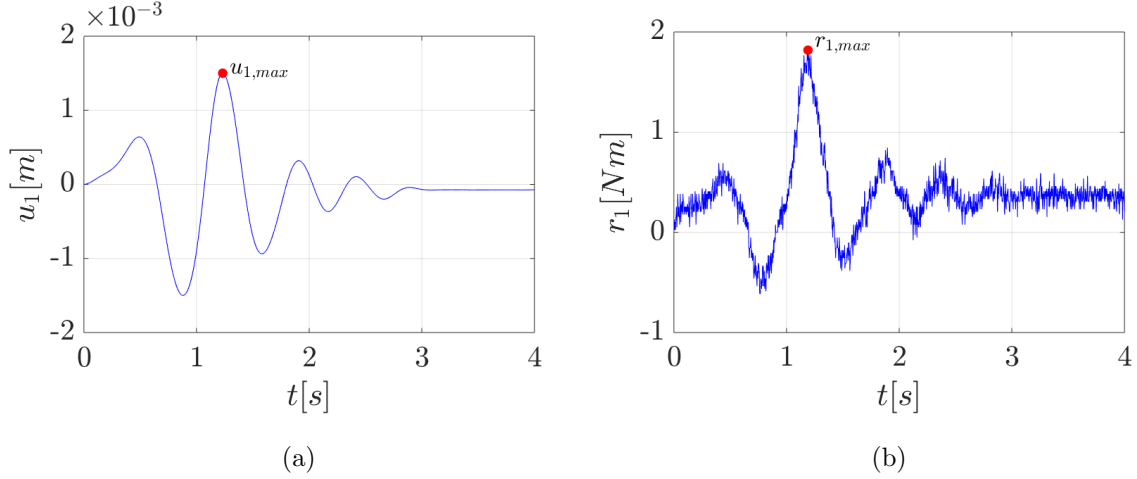
14

Figure 5: Outcomes of a sample HS of the response of the hybrid model of the prototype structure with $K_1 = K_2 = 70\,\mathrm{Nm/rad}$ to a velocity-pulse ground motion excitation with $V_P = 2\,\mathrm{m/s}$, $T_P = 1.25\,\mathrm{s}$ in terms of left support rotation (a) and bending moment (b) response histories. QoIs are highlighted.
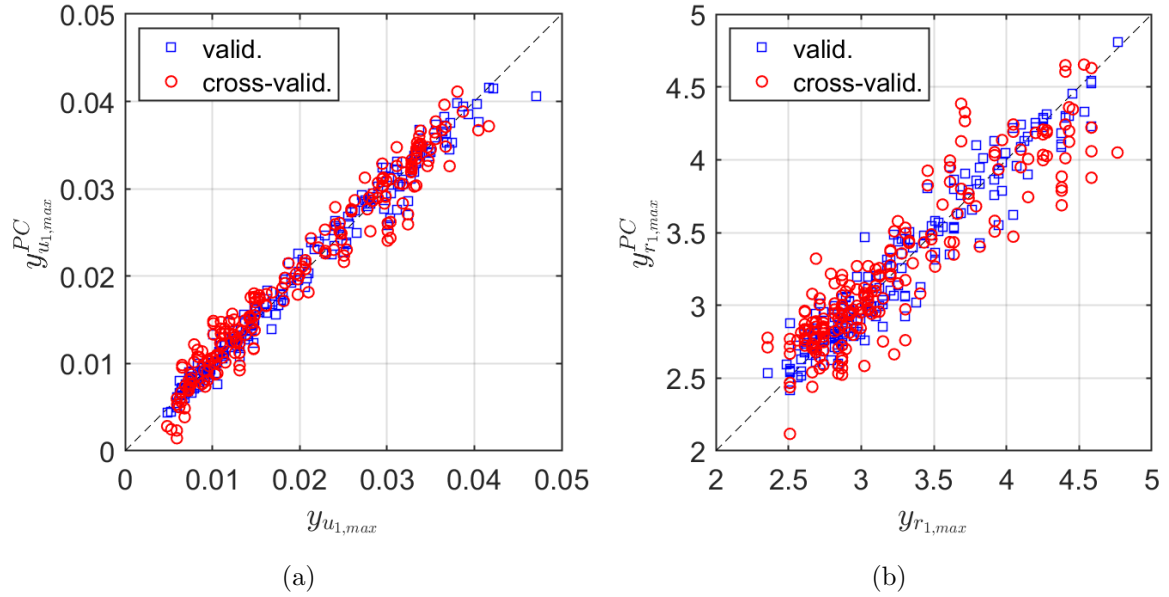

Figure 6: Relationship between QoI measurements and corresponding PCE estimates for (a) $u_{1,\mathrm{max}}$ and (b) $r_{1,\mathrm{max}}$.

PCEs. Notably, the higher noise floor of response r_1 produces a more remarkable dispersion on QoI $r_{1,\mathrm{max}}$. Figure 7 shows the convergence of LOO errors of both PCEs computed considering EDs of increasing size from 10 to 200 samples. It is worth noting that force measurement noise and displacement control errors are both sources of aleatory uncertainty that propagate through
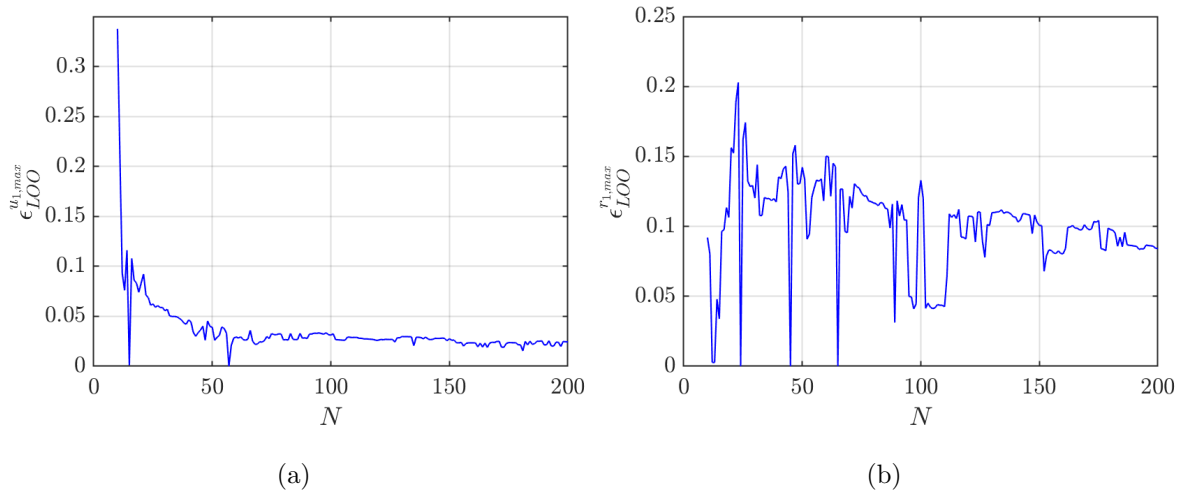
15

Figure 7: Convergence of LOO error estimates of (a) $u_{1,\max}$ and (b) $r_{1,\max}$ PCEs.

the hybrid model response, which is inherently stochastic. In this case, PCE acts as a data denoiser, and for this reason, LOO errors do not converge to zero. Figures 8 and 9 show the convergence plots of the mean, variance and CoV PCE-based estimates for both QoIs. Evidently, all PCE estimates converge in a stable manner, with reliable values attained for ED sizes larger than 50 samples.
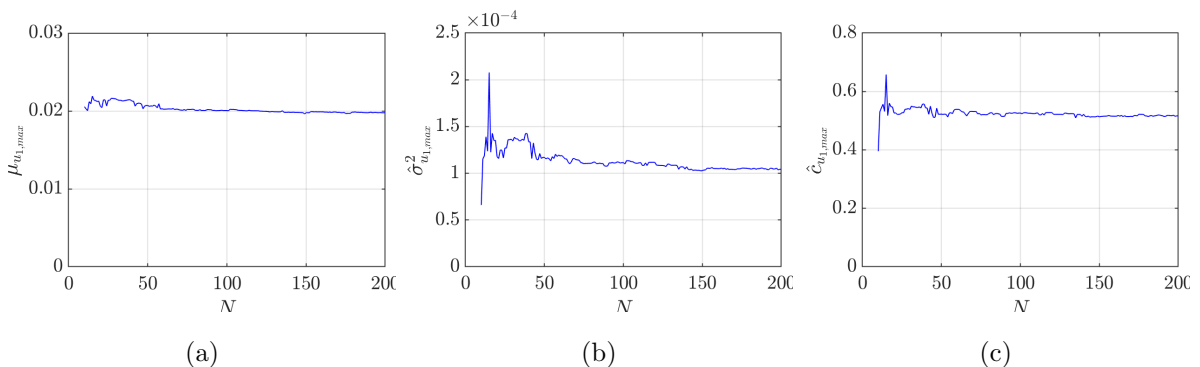

Figure 8: Convergence of PCE estimates of (a) mean, (b) variance and (c) CoV of QoI $u_{1,\max}$.

4.2 GSA based on Sobol' sensitivity indices

Based on PCEs of both QoIs, Sobol' indices are obtained as explained in Subsection 2.2. Figure 10 reports first-order and total Sobol' indices for QoIs $u_{1,\max}$ and $r_{1,\max}$. The error bars are computed from 50 bootstrap replications of the underlying PCE (Dubreuil et al., 2014), and demonstrate that the accuracy of the surrogate is appropriate for this application. According to
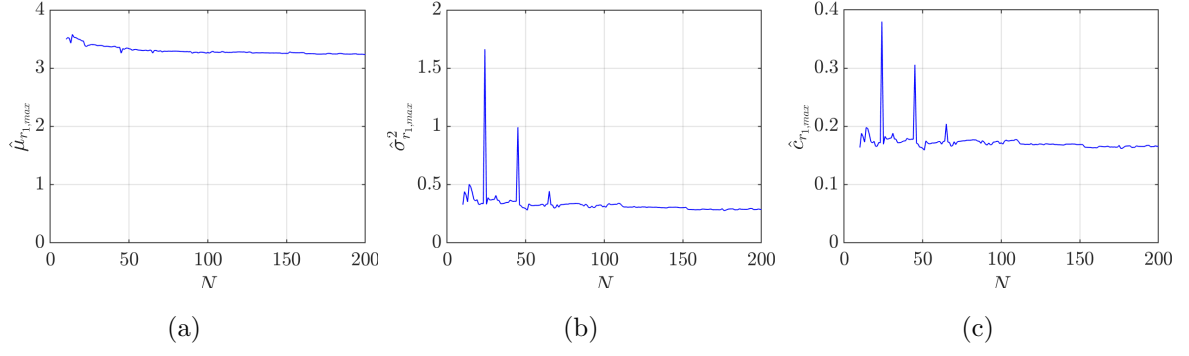
Figure 9: Convergence of PCE estimates of (a) mean, (b) variance and (c) CoV of QOI $r_{1,\max}$.
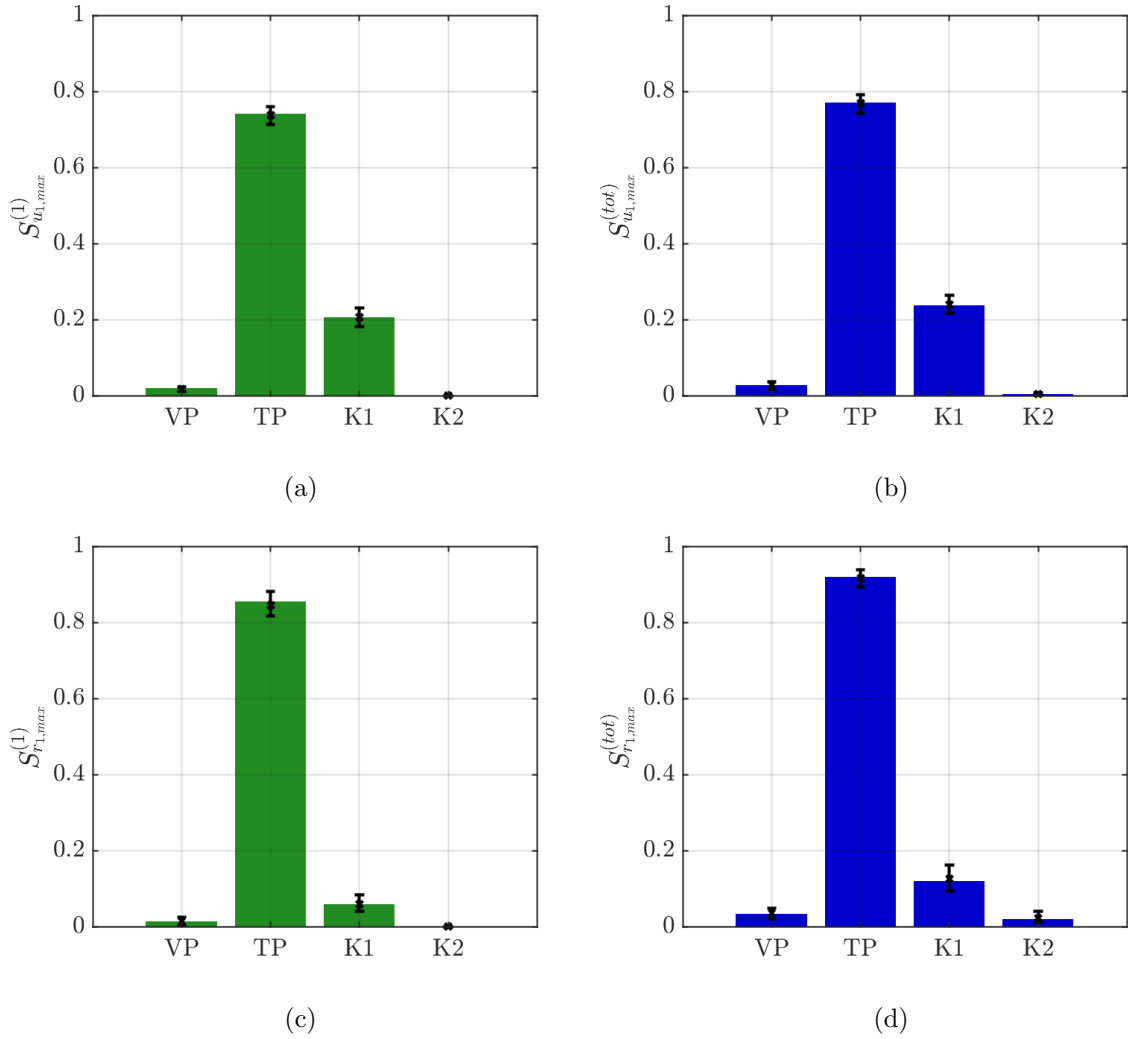

Figure 10: First-order and total Sobol' indices for (a-b) $u_{1,\max}$ and (c-d) $r_{1,\max}$ PCEs.

Figure 10, the period T_p of the velocity pulse and the stiffness K_1 of the left torsional spring are the most sensitive input variables for both QoIs. This result finds an intuitive explanation. The

17

range of velocity-pulse period T_p was selected to cross the range of periods of the first bending mode of the hybrid model, given the range of the stiffness of the rotation springs. Further, rotation spring stiffness K_1 is a boundary condition at the left edge of the PS iron plate, corresponding to responses u_1 and r_1. Therefore, QoIs are expected to be more sensitive to K_1 than K_2. It should be noted that the bending stiffness of the plate specimen has the same order of magnitude as the maximum stiffness value of the left-support rotation spring K_1 (see Table 1), thus a fixed boundary configuration, which would heavily affect the response of the plate, was not approached in this case study. It is, indeed, reasonable from the standpoint of resonance that the velocity-pulse period T_P has more influence on the prototype structure response than K_1, and significantly more influence than the velocity pulse amplitude V_P. Finally, the small difference between pairs of first-order and total Sobol' indices indicates that the high-order interactions among input variables are negligible.

In order to provide further insight into the prototype structure response, univariate effects are reported in Figure 11 for input variables T_P and K_1, to which the response of the prototype structure is the most sensitive, as highlighted by the GSA. Evidently, univariate effects decrease monotonically for PCEs of both QoIs over the ranges of the two considered input variables.

5   Conclusions

A Global Sensitivity Analysis (GSA) framework for Hybrid Simulation (HS) was presented in this paper. The proposed framework, based on Sobol' sensitivity indices, is intended to quantify the fraction of the variability of a generic response quantity of interest (QoI) of the prototype structure due to the variability of a set of input variables that provide a suitable parametrization of the prototype structure and the excitation. The response of the prototype structure is evaluated using HS, thus involving a hybrid model comprised of a few Physical Substructures (PSs) tested in laboratory test setups, and a potentially large number of Numerical Substructures (NSs), emulated using computer models. Such an approach provides for a more realistic evaluation of the response of the prototype structure but still precludes the conduct of a large number of tests due to cost and time considerations. To resolve this issue, Polynomial Chaos Expansion (PCE) was used to surrogate the hybrid model response. Thereafter, Sobol' sensitivity indices were obtained as a by-product of polynomial coefficients, entailing a reduced number of HSs compared to a crude Monte Carlo approach to achieve the same quality of response sensitivity estimates. A case study characterized by four uncertain input variables, two of which related to the NS while the other two related to the excitation, was used to
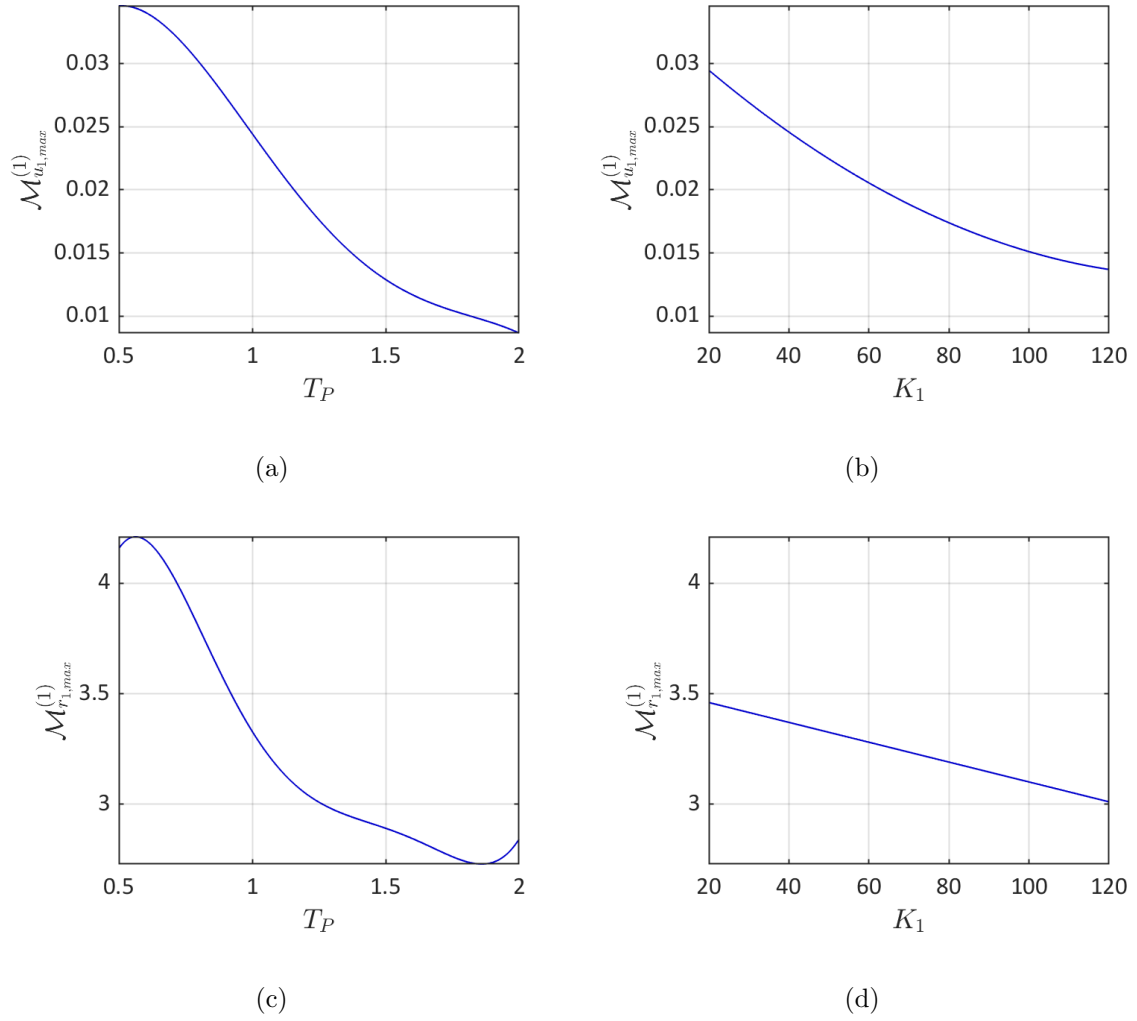
Figure 11: Univariate effects on PCEs for (a-b) $u_{1,\max}$ and (c-d) $r_{1,\max}$.

validate the proposed framework. As a general observation, the noise floor of each response QoI of the prototype structure, which is determined by random experimental errors entailed in HS, prevents the generalization error of the corresponding PCE to converge to zero asymptotically. In the case of a soft specimen, such as the one used in the case study, displacement-based QoIs are less noisy than force-based QoIs. However, stable plateau values indicate that PCE acts as a powerful denoiser and, therefore, is very well-suited to surrogate the hybrid model response, making the proposed GSA framework for HS possible. Stable PCEs and, hence, stable Sobol' sensitivity indices, were available with as few as 50 HSs in the conducted case study. Several such HSs can be easily afforded when the PSs of the hybrid model can sustain repeated experiments without deteriorating appreciably (e.g. seismic isolation bearings). However, when the PSs accumulate damage during HS and need to be replaced experiment after experiment, several

such HSs might not be affordable. Therefore, future work should aim to reduce the number of HSs necessary to achieve stable convergence of PCEs by, for example, employing adaptive sampling strategies to build the ED. In this situation, a better understanding of the propagation of the parasitic inter-specimen variability of the PS response throughout the estimation of Sobol' sensitivity indices is also needed. Fundamentally, the findings presented in this paper indicate that experimental campaigns designed according to the current earthquake engineering practice and, therefore, relying on a few HSs with degrading PSs, can only provide *qualitative* instead of *quantitative* information about the structural sensitivity of the prototype structure response. Yet, quantifying the response sensitivity is very valuable, both in terms of planning additional HSs for model validation and verification, and in terms of modeling and analysis choices in the overall structural design process. This motivates our continuing work.

Appendix A. Time integration algorithm for hybrid simulation

A partitioned time integration algorithm tailored to state-space equations of motion computes the time history response of the hybrid model in a HS. The state-space formulation of the equation of motion of a generic mechanical system reads:

$$\mathbf{M}\dot{\mathbf{Y}} + \mathbf{R}\left(\mathbf{Y}\right) = \mathbf{F}\left(t\right) \tag{A.1}$$

with,

$$\mathbf{Y} = \begin{bmatrix} \mathbf{u} \\ \mathbf{v} \\ \mathbf{s} \end{bmatrix}, \mathbf{M} = \begin{bmatrix} \mathbf{I} & \mathbf{0} & \mathbf{0} \\ \mathbf{0} & \mathbf{m} & \mathbf{0} \\ \mathbf{0} & \mathbf{0} & \mathbf{I} \end{bmatrix}, \mathbf{R} = \begin{bmatrix} -\mathbf{v} \\ \mathbf{r}\left(\mathbf{u}, \mathbf{v}, \mathbf{s}\right) \\ \mathbf{g}\left(\mathbf{u}, \mathbf{v}, \mathbf{s}\right) \end{bmatrix}, \mathbf{F}\left(t\right) = \begin{bmatrix} \mathbf{0} \\ \mathbf{f}\left(t\right) \\ \mathbf{0} \end{bmatrix} \tag{A.2}$$

where vectors $\mathbf{u}$, $\mathbf{v}$ and $\mathbf{s}$ contain displacement, velocity and additional state variables, respectively. The former two vectors always appear as a pair in second-order mechanical systems, while the latter is used to model nonlinearities endowed with memory, e.g. hysteresis. In particular, $\mathbf{r}(\mathbf{u}, \mathbf{v}, \mathbf{s})$ is the nonlinear restoring force vector while $\mathbf{g}(\mathbf{u}, \mathbf{v}, \mathbf{s})$ is a nonlinear function that describes the evolution of additional state variables $\mathbf{s}$; $\mathbf{m}$ is the mass matrix and $\mathbf{f}(t)$ is the external time varying load, while $\mathbf{I}$ and $\mathbf{0}$ are identity and zero matrices, respectively. When (A.1)-(A.2) refer to a linear system, no additional state variable $\mathbf{s}$ enters the state vector $\mathbf{Y}$ and the restoring force is defined as:

$$\mathbf{r}\left(\mathbf{u}, \mathbf{v}\right) = \mathbf{k}\mathbf{u} + \mathbf{c}\mathbf{v} \tag{A.3}$$

where $\mathbf{k}$ and $\mathbf{c}$ are stiffness and damping matrices, respectively. For the sake of simplicity, time dependency is omitted hereafter while $\mathbf{M}$, $\mathbf{K}$, $\mathbf{R}$ and $\mathbf{F}$ are referred to as generalized mass, stiffness, restoring force and external loading.

The partitioned time integration algorithm, which adopts the dual assembly strategy of the modified Prakash-Hjelmstad method Brun et al. (2014), synchronizes two monolithic time integration processes characterized by different time steps. In detail, a set of Lagrange multipliers enforces compatibility of PS and NS interface velocities at the coarser time step. The corresponding coupled system of equations of motion reads:

$$
\begin{cases}
\mathbf{M}^N \dot{\mathbf{Y}}_{k+1}^N + \mathbf{R}^N \left(\mathbf{Y}_{k+1}^N \right) = \mathbf{F}_{k+1}^N + \mathbf{B}^{N^T} \mathbf{\Lambda}_{k+1} \\
\mathbf{M}^P \dot{\mathbf{Y}}_{k+\frac{j}{m}}^P + \mathbf{R}^P \left(\mathbf{Y}_{k+\frac{j}{m}}^P \right) = \mathbf{F}_{k+\frac{j}{m}}^P + \mathbf{B}^{P^T} \left(\frac{m-j}{m} \mathbf{\Lambda}_k + \frac{j}{m} \mathbf{\Lambda}_{k+1} \right) \\
\mathbf{G}^N \dot{\mathbf{Y}}_{k+1}^N + \mathbf{G}^P \dot{\mathbf{Y}}_{k+1}^P = \mathbf{0}
\end{cases}
\tag{A.4}
$$

where signed Boolean collocation matrices $\mathbf{B}$ and $\mathbf{G}$ localize interface forces and define compatibility equations, respectively, and are defined as:

$$
\mathbf{B} = \begin{bmatrix} \mathbf{0} & \mathbf{l} & \mathbf{0} \end{bmatrix}, \mathbf{G} = \begin{bmatrix} \mathbf{l} & \mathbf{0} & \mathbf{0} \end{bmatrix}
\tag{A.5}
$$

Boolean collocation matrices $\mathbf{l}$ localize interface DoF pairs across NS and PS. In principle, at each simulation step, the computation of the state vector (A.4) is split into *free* and *link* solutions. The *coupled* solution is the sum of *free* and *link* contributions. According to (A.4)-(A.5), two parameters define the setting of the algorithm,

- testing time scale λ, defined as $\lambda = \frac{\Delta t^C}{\Delta t^P} = \frac{\Delta t^S}{\Delta t^N}$

- subcycling m, defined as $m = \frac{\Delta t^N}{\Delta t^P} = \frac{\Delta t^S}{\Delta t^C}$

Time steps Δt^N and Δt^P refer to simulation time, which is the virtual time axis defined by the time integration process. As an example, the seismic ground motion history refers to the simulation time axis. In particular, Δt^N is the time step adopted for integrating the NS response while Δt^P refers to the PS. On the other hand, Δt^S and Δt^C refer to wall-clock time measured in the laboratory. The former, Δt^S, defines the maximum solving time allocated to compute the NS response while the latter, Δt^C, is the actuator controller time step, which typically ranges between 1 and 2 msec. In order to minimize discontinuity of actuator trajectories, the PS equation should be evaluated within a single controller time step Δt^C.

The testing time scale λ defines the ratio between wall-clock and simulation time rates. In particular, $\lambda = 1$ corresponds to real-time HS. If $\lambda > 1$, the simulation time flow is slower than the wall-clock time. This case corresponds to the pseudodynamic HS regime. When the response of the PS is not rate-dependent, λ usually ranges between 50 and 200. This approach reduces displacement tracking errors as well as the destabilizing effect of actuator delay, which typically

ranges from 10 to 20 msec. The subcycling parameter m allows for adjusting Δt^S, which is the fixed time window allocated for solving the NS response. Accordingly, optimal tuning of testing time scale λ and subcycling m is a trade-off between computational accuracy and experimental capacity. For a detailed description of the partitioned time integration algorithm, the reader should refer to Abbiati et al. (2019).

Acknowledgments

References

References

Abbiati, G., V. Hey, J. Rion, and B. Stojadinovic (2018). Thermo-mechanical virtualization of hybrid flax/carbon fiber composite for spacecraft structures. thermics project, final report.

Abbiati, G., V. La Salandra, O. S. Bursi, and L. Caracoglia (2018, 2). A composite experimental dynamic substructuring method based on partitioned algorithms and localized Lagrange multipliers. *Mechanical Systems and Signal Processing 100*, 85–112.

Abbiati, G., I. Lanese, E. Cazzador, O. S. Bursi, and A. Pavese (2019, 7). A computational framework for fast-time hybrid simulation based on partitioned time integration and state-space modeling. *Structural Control and Health Monitoring* (June), 1–28.

Ahmadizadeh, M. and G. Mosqueda (2009). Online energy-based error indicator for the assessment of numerical and experimental errors in a hybrid simulation. *Eng. Struct. 31*(9), 1987–1996.

Becker, T. S., D. J. Van Manen, C. M. Donahue, C. Bärlocher, N. Börsing, F. Broggini, T. Haag, J. O. Robertsson, D. R. Schmidt, S. A. Greenhalgh, and T. E. Blum (2018). Immersive Wave Propagation Experimentation: Physical Implementation and One-Dimensional Acoustic Results. *Physical Review X 8*(3), 31011.

Berveiller, M., B. Sudret, and M. Lemaire (2006, 1). Stochastic finite element: a non intrusive approach by regression. *European Journal of Computational Mechanics 15*(1-3), 81–92.

Blatman, G. and B. Sudret (2011, 3). Adaptive sparse polynomial chaos expansion based on least angle regression. *Journal of Computational Physics 230*(6), 2345–2367.

Bradley, B. A. (2013, 9). A critical examination of seismic response uncertainty analysis in earthquake engineering. *Earthquake Engineering & Structural Dynamics 42*(11), 1717–1729.

Brun, M., A. Batti, A. Combescure, and A. Gravouil (2014, 9). External coupling software based on macro- and micro-time scales for explicit/implicit multi-time-step co-computations in structural dynamics. *Finite Elements in Analysis and Design 86*, 101–119.

Bursi, O. S., G. Abbiati, E. Cazzador, P. Pegon, and F. J. Molina (2017, 11). Nonlinear heterogeneous dynamic substructuring and partitioned FETI time integration for the development of low-discrepancy simulation models. *International Journal for Numerical Methods in Engineering 112*(9), 1253–1291.

Christenson, R., Y. Z. Lin, A. Emmons, and B. Bass (2008). Large-Scale Experimental Verification of Semiactive Control through Real-Time Hybrid Simulation. *Journal of Structural Engineering 134*(4), 522–534.

Dabaghi, M. and A. Der Kiureghian (2018, 5). Simulation of orthogonal horizontal components of near-fault ground motion for specified earthquake source and site characteristics. *Earthquake Engineering & Structural Dynamics 47*(6), 1369–1393.

Deman, G., K. Konakli, B. Sudret, J. Kerrou, P. Perrochet, and H. Benabderrahmane (2016). Using sparse polynomial chaos expansions for the global sensitivity analysis of groundwater lifetime expectancy in a multi-layered hydrogeological model. *Reliab. Eng. Sys. Safety 147*, 156–169.

Dubreuil, S., M. Berveiller, F. Petitjean, and M. Salaün (2014). Construction of bootstrap confidence intervals on sensitivity indices computed by polynomial chaos expansion. *Reliability Engineering & System Safety 121*, 263–275.

Franza, A. and A. M. Marshall (2018). Centrifuge and Real-Time Hybrid Testing of Tunneling beneath Piles and Piled Buildings. *Journal of Geotechnical and Geoenvironmental Engineering* (3), 04018110.

Harenberg, D., S. Marelli, B. Sudret, and V. Winschel (2019). Uncertainty quantification and global sensitivity analysis for economic models. *Quantitative Economics 10*(1), 1–41.

Le Gratiet, L., S. Marelli, and B. Sudret (2017). Metamodel-Based Sensitivity Analysis: Polynomial Chaos Expansions and Gaussian Processes. In *Handbook of Uncertainty Quantification*, pp. 1289–1325. Cham: Springer International Publishing.

Marelli, S., C. Lamas, K. Konakli, C. Mylonas, P. Wiederkehr, and B. Sudret (2019). UQLab user manual – Sensitivity analysis. Technical report, Chair of Risk, Safety & Uncertainty Quantification, ETH Zurich. Report # UQLab-V1.2-106.

Marelli, S. and B. Sudret (2014, 6). UQLab: A Framework for Uncertainty Quantification in Matlab. In *Vulnerability, Uncertainty, and Risk*, pp. 2554–2563. American Society of Civil Engineers.

Marelli, S. and B. Sudret (2019). UQLab user manual – Polynomial chaos expansions. Technical report, Chair of Risk, Safety & Uncertainty Quantification, ETH Zurich. Report # UQLab-V1.2-104.

Saltelli, A., M. Ratto, T. Andres, F. Campolongo, J. Cariboni, D. Gatelli, M. Saisana, and S. Tarantola (2007, 12). *Global Sensitivity Analysis. The Primer*, Volume 76. Chichester, UK: John Wiley & Sons, Ltd.

Sauder, T., S. Marelli, K. Larsen, and A. J. Sørensen (2018, 5). Active truncation of slender marine structures: Influence of the control system on fidelity. *Applied Ocean Research 74*, 154–169.

Shellenberg A.H., Mahin S.A., F. G. (2009). Advanced Implementation of Hybrid Simuation. Technical Report 104, Pacific Earthquake Engineering Research Center.

Sobol', I. M. (1993). Sensitivity Estimates for Nonlinear Mathematical Models. Technical report.

Sudret, B. (2008, 7). Global sensitivity analysis using polynomial chaos expansions. *Reliability Engineering & System Safety 93*(7), 964–979.

Terzic, V., B. Stojadinovic, and M. Asce (2014). Hybrid Simulation of Bridge Response to Three-Dimensional Earthquake Excitation Followed by Truck Load. *Journal of Structural Engineering 140*(8), A4014010.

Torre, E., S. Marelli, P. Embrechts, and B. Sudret (2019, 7). Data-driven polynomial chaos expansion for machine learning regression. *Journal of Computational Physics 388*, 601–623.

Vasmel, M., J. O. A. Robertsson, D.-J. van Manen, and A. Curtis (2013). Immersive experimentation in a wave propagation laboratory. *The Journal of the Acoustical Society of America 134*(6), EL492–EL498.

Whyte, C. A., K. R. Mackie, and B. Stojadinovic (2016, 2). Hybrid Simulation of Thermomechanical Structural Response. *Journal of Structural Engineering 142*(2), 04015107.

Xiu, D. and G. E. Karniadakis (2002, 1). The Wiener–Askey Polynomial Chaos for Stochastic Differential Equations. *SIAM Journal on Scientific Computing 24*(2), 619–644.